Electronic Supplementary Material (ESI) for Soft Matter.
This journal is © The Royal Society of Chemistry 2019

©The Royal Society of Chemistry 2019

Electronic Supplementary Information (ESI) for Soft Matter: *Transition rates for slip-avalanches in soft athermal disks under quasi-static simple shear deformations*

Kuniyasu Saitoh [*,†], Norihiro Oyama [‡], Fumiko Ogushi [§,¶], and Stefan Luding [‖]

February 25, 2019

1 Affine responses of contact force and angle

In this section, we derive the affine responses of contact force and angle to simple shear deformation.

As shown in Fig. 1, the relative position between the disks, i and j, is changed from $\mathbf{r}_{ij} = (r_{ijx}, r_{ijy})$ to $\mathbf{r}'_{ij} = (r'_{ijx}, r'_{ijy}) = (r_{ijx} + \Delta\gamma r_{ijy}, r_{ijy})$ by the strain step, $\Delta\gamma$. In first order approximation of $\Delta\gamma$, the interparticle distance, $r_{ij} = \sqrt{r_{ijx}^2 + r_{ijy}^2}$, changes to

$$\begin{aligned} r'_{ij} &= \sqrt{r'^2_{ijx} + r'^2_{ijy}} \\ &\simeq r_{ij}\left(1 + \Delta\gamma n_{ijx} n_{ijy}\right) \\ &= r_{ij}\left(1 + \frac{\Delta\gamma}{2}\sin 2\theta_{ij}\right) , \end{aligned} \tag{1}$$

where $\mathbf{n}_{ij} = \mathbf{r}_{ij}/r_{ij} = (n_{ijx}, n_{ijy}) = (\cos\theta_{ij}, \sin\theta_{ij})$ is the unit vector parallel to the relative position (before deformation). Thus, the force change, $\Delta f^{\mathrm{a}}_{ij} \equiv f^{\mathrm{a}}_{ij} - f_{ij} = k(r_{ij} - r'_{ij})$, is given by

$$\Delta f^{\mathrm{a}}_{ij} \simeq -\frac{\Delta\gamma}{2} k r_{ij} \sin 2\theta_{ij} . \tag{2}$$

In Fig. 1, we find $r_{ij}/\sin\theta^{\mathrm{a}}_{ij} = \Delta\gamma r_{ijy}/\sin(-\Delta\theta^{\mathrm{a}}_{ij})$ from the sine rule. If we use $(r_{ijy}/r_{ij})\sin\theta^{\mathrm{a}}_{ij} = \sin\theta_{ij}\sin\theta^{\mathrm{a}}_{ij} = \left\{\cos(\Delta\theta^{\mathrm{a}}_{ij}) - \cos(\theta^{\mathrm{a}}_{ij} + \theta_{ij})\right\}/2$, it is readily found that

$$\sin(\Delta\theta^{\mathrm{a}}_{ij}) = \frac{\Delta\gamma}{2}\left\{\cos(\theta^{\mathrm{a}}_{ij} + \theta_{ij}) - \cos(\Delta\theta^{\mathrm{a}}_{ij})\right\} . \tag{3}$$

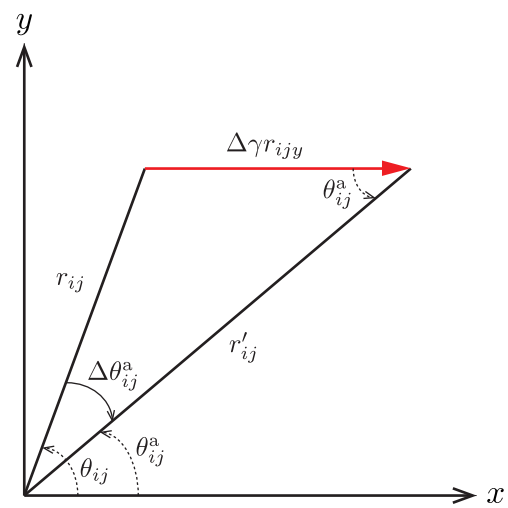

Figure 1: A sketch of interparticle distances before and after simple shear deformation, r_{ij} and r'_{ij}, respectively. The angle θ_{ij} changes to θ^{a}_{ij}, where $\Delta\theta^{\mathrm{a}}_{ij} \equiv \theta^{\mathrm{a}}_{ij} - \theta_{ij}$.

Because the strain step is small, we can assume $\Delta\theta^{\mathrm{a}}_{ij} \ll 1$, where $\sin(\Delta\theta^{\mathrm{a}}_{ij}) \simeq \Delta\theta^{\mathrm{a}}_{ij}$, $\cos(\theta^{\mathrm{a}}_{ij} + \theta_{ij}) \simeq \cos 2\theta_{ij}$, and $\cos(\Delta\theta^{\mathrm{a}}_{ij}) \simeq 1$. Then, Eq. (3) is reduced to

$$\Delta\theta^{\mathrm{a}}_{ij} \simeq \frac{\Delta\gamma}{2}(\cos 2\theta_{ij} - 1) . \tag{4}$$

Equation (4) includes the frame rotation (*vorticity*), $\varphi = -\Delta\gamma/2$; thus we subtract φ from $\Delta\theta^{\mathrm{a}}_{ij}$ to find the objective (frame independent) change of contact angle:

$$\Delta\theta^{\mathrm{a}}_{ij} - \varphi = \frac{\Delta\gamma}{2}\cos 2\theta_{ij} . \tag{5}$$

2 Non-affine responses of contact angle

In this section, we show the non-affine responses of the contact angle, $\Delta\theta_{ij}$.

[*]Research Alliance Center for Mathematical Sciences, Tohoku University, 2-1-1 Katahira, Aoba-ku, Sendai 980-8577, Japan.
[†]WPI-Advanced Institute for Materials Research, Tohoku University, 2-1-1 Katahira, Aoba-ku, Sendai 980-8577, Japan.
[‡]Mathematics for Advanced Materials-OIL, AIST-Tohoku University, Sendai 980-8577, Japan.
[§]Center for Materials research by Information Integration, National Institute for Materials Science, 1-2-1 Sengen, Tsukuba, Ibaraki 305-0047, Japan.
[¶]Kyoto University Institute for Advanced Study, Kyoto University, Yoshida Ushinomiya-cho, Sakyo-ku, Kyoto, 606-8501, Japan.
[‖]Faculty of Engineering Technology, MESA+, University of Twente, Drienerlolaan 5, 7522 NB, Enschede, The Netherlands.

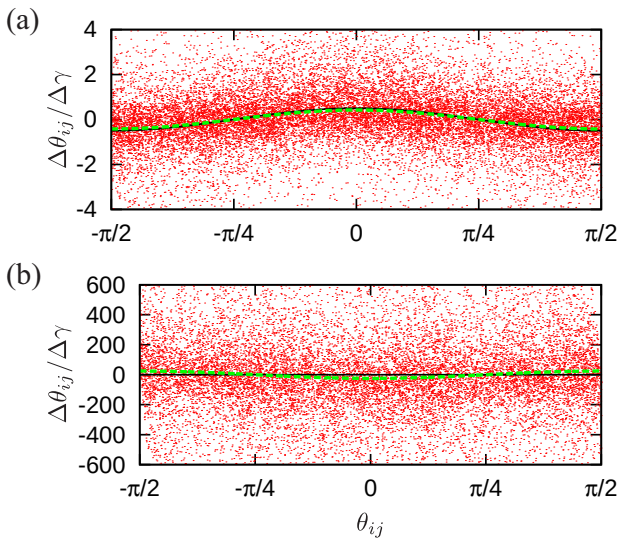

Figure 2: Scatter plots of the scaled angle change, $\Delta\theta_{ij}/\Delta\gamma$, and contact angle, θ_{ij}, where we observe linear increase of shear stress in (a) and slip-avalanche in (b). The solid lines represent Eq. (5), while the dashed lines are the fits to data, $A\cos(2\theta_{ij})$, where $A = 0.422$ (a) and -24.4 (b). The area fraction is $\phi = 0.9$. Note the different vertical scales in (a) and (b).

Figure 2 displays scatter plots of the scaled angle change, $\Delta\theta_{ij}/\Delta\gamma$, for increase of stress and a slip event. In this figure, the solid lines represent the affine prediction, Eq. (5), while the dashed lines are the fits, $A\cos(2\theta_{ij})$, to data (the dots).

3 Numerical calculation of transition rates

In this section, we explain how to calculate the *transition rate* of contact forces and angles from numerical data. Here, we omit the subscripts, ij, from the contact force and angle, f_{ij} and θ_{ij}.

First, we make a histogram of contact force and angle as $\mathrm{hist}[f,\theta]$, where the bin sizes (or small increments) of contact force and angle are introduced as df and $d\theta$, respectively. Then, the *probability distribution function* (PDF) of contact force and angle is calculated as

$$P_\gamma(f,\theta) = \frac{\mathrm{hist}[f,\theta]}{N_p df d\theta}\,, \tag{6}$$

where N_p is the total number of contacts. Because the total number of contacts is given by

$$N_p = \sum_f \sum_\theta \mathrm{hist}[f,\theta]\,, \tag{7}$$

the PDF defined in Eq. (6) satisfies the normalization condition, $\iint P_\gamma(f,\theta) df d\theta = 1$. Similarly, the PDF after applying the strain step, $\Delta\gamma$, is calculated as

$$P_{\gamma+\Delta\gamma}(f',\theta') = \frac{\mathrm{hist}[f',\theta']}{N_p df' d\theta'}\,, \tag{8}$$

where df' and $d\theta'$ are small increments of contact force and angle after the strain step. Note that the number of contacts can decrease (increase) by opening (closing) contacts, which we neglected in Eq. (8). The complete statistics is subject to ongoing research and will be published elsewhere.

Next, we make a histogram of f' and θ', which were f and θ before applying the strain step, as $\mathrm{hist}[f',\theta'|f,\theta]$. The histogram satisfies the relations

$$\sum_f \sum_\theta \mathrm{hist}[f',\theta'|f,\theta] = \mathrm{hist}[f',\theta']\,, \tag{9}$$

$$\sum_{f'} \sum_{\theta'} \mathrm{hist}[f',\theta'|f,\theta] = \mathrm{hist}[f,\theta]\,. \tag{10}$$

Then, the *conditional probability distribution* (CPD) is defined as

$$W(f',\theta'|f,\theta) = \frac{\mathrm{hist}[f',\theta'|f,\theta]}{\mathrm{hist}[f,\theta] df' d\theta'}\,, \tag{11}$$

which is normalized as

$$\begin{aligned}\iint W(f',\theta'|f,\theta) df' d\theta' &= \sum_{f'} \sum_{\theta'} \frac{\mathrm{hist}[f',\theta'|f,\theta]}{\mathrm{hist}[f,\theta] df' d\theta'} df' d\theta' \\ &= 1\,,\end{aligned} \tag{12}$$

where we used Eq. (10). From Eqs. (6), (8), (9), and (11), we find

$$\begin{aligned}&\iint W(f',\theta'|f,\theta) P_\gamma(f,\theta) df d\theta \\ &= \sum_f \sum_\theta \frac{\mathrm{hist}[f',\theta'|f,\theta]}{\mathrm{hist}[f,\theta] df' d\theta'} \frac{\mathrm{hist}[f,\theta]}{N_p df d\theta} df d\theta \\ &= \sum_f \sum_\theta \frac{\mathrm{hist}[f',\theta'|f,\theta]}{N_p df' d\theta'} \\ &= \frac{\mathrm{hist}[f',\theta']}{N_p df' d\theta'} \\ &= P_{\gamma+\Delta\gamma}(f',\theta')\,,\end{aligned} \tag{13}$$

which is the *Chapman-Kolmogorov equation* of the PDFs, i.e.

$$P_{\gamma+\Delta\gamma}(f',\theta') = \iint W(f',\theta'|f,\theta) P_\gamma(f,\theta) df d\theta\,. \tag{14}$$

Introducing the transition rate of contact force and angle as

$$T(f',\theta'|f,\theta) \equiv \lim_{\Delta\gamma\to 0} \frac{W(f',\theta'|f,\theta)}{\Delta\gamma}\,, \tag{15}$$

we can derive the *master equation* of the PDFs (Eq. (2) in main text) from the Chapman-Kolmogorov equation (14).

4 Angular dependence of transition rates

In this section, we discuss the dependence of the transition rates on the contact angles, θ and θ'.

As shown in the main paper, the transition rate is approximated very well by the q-Gaussian distribution,

$$T(\mathbf{f}|\mathbf{f}') = C_q \frac{c(\Delta\theta)}{w(\Delta\theta)} \left[1 + (q-1) \left\{ \frac{\Delta f - \langle \Delta f \rangle}{w(\Delta\theta)} \right\}^2 \right]^{-\frac{1}{q-1}} . \quad (16)$$

First, the transition rates are independent of the initial angle, θ. Figure 3 displays the transition rates for slip-avalanches, where the angle change is zero, $\Delta\theta = \theta - \theta' = 0$. As can be seen, all the data are fairly well fitted by the same q-Gaussian distribution, Eq. (16) (solid lines), regardless of the contact angles, $\theta = \theta'$, and area fraction of the disks, ϕ. Here, the same parameters, $q = 2.45$, $c(0) = 5.29$, and $w(0) = 7.06 \times 10^{-5}$, are used for all the data, though the smallest ϕ shows the most disagreement in the tail.

Second, the transition rates monotonously decrease with the increase of angle change, $\Delta\theta$. Figure 4(a) shows the transition rates for slip-avalanches, where $\Delta\theta \neq 0$. The lines are the q-Gaussian distributions, Eq. (16), where the dependence on angle change, $\Delta\theta$, is well captured by the parameters, $c(\Delta\theta)$ and $w(\Delta\theta)$, as in Fig. 4(b).

Last, the transition rates, Eq. (16), are functions of force change, Δf, and angle change, $\Delta\theta$, and are shown as a three-dimensional plot in Fig. 5. Here, the q-index, $w(\Delta\theta)$, and $c(\Delta\theta)$ are as in Figs. 3 and 4. As can be seen, the transition rate (scaled by $c(\Delta\theta)$) has a sharp peak around $(\Delta f, \Delta\theta) = (\langle \Delta f \rangle, 0)$. It gradually decreases with the increase of Δf and $\Delta\theta$ such that drastic changes of contact force and angle are rare.

5 Avalanche-size distributions

In this section, we summarize our results of *probability distribution functions* (PDFs) of avalanche-sizes. First, we derive a relation between the PDFs and transition rates (Sec. 5.1). Then, we discuss the dependence of the PDFs on the area fraction (Sec. 5.2) and system size (Sec. 5.3).

5.1 Connection to transition rates

The virial expression, or *microscopic expression*, of the stress drop amplitude is given by

$$\Delta\sigma = \frac{1}{2L^2} \iint f r \sin 2\theta \Delta P(\mathbf{f}) d\mathbf{f} , \quad (17)$$

where $\Delta P(\mathbf{f})$ is the change of the PDF of contact forces and angles. On the other hand, the ensemble average of the stress drop is written as

$$\langle \Delta\sigma \rangle = \int \Delta\sigma P(\Delta\sigma) d\Delta\sigma , \quad (18)$$

where $P(\Delta\sigma)$ is introduced as the PDF of the stress drop. Here, Eq. (18) is a *macroscopic expression* of the stress drop amplitude. Substituting Eq. (17) into the left-hand-side of Eq. (18), we find

$$\begin{aligned} & \int \Delta\sigma P(\Delta\sigma) d\Delta\sigma \\ = & \left\langle \frac{1}{2L^2} \iint f r \sin 2\theta \left[T(\mathbf{f}|\mathbf{f}') P(\mathbf{f}') - T(\mathbf{f}'|\mathbf{f}) P(\mathbf{f}) \right] \Delta\gamma d\mathbf{f} d\mathbf{f}' \right\rangle , \end{aligned} \quad (19)$$

where the master equation (Eq. (2) in the main paper) is used for the change of the PDF, $\Delta P(\mathbf{f})$. Equation (19) is the relation between micro- and macroscopic expressions of $\Delta\sigma$, connecting the microscopic contact forces and angles with the macroscopic stress-drop amplitudes.

5.2 Dependence on the area fraction

We show the dependence of avalanche-size distributions on the area fraction. Here, the avalanche-size is defined as an extensive quantity,

$$S \equiv L^2 \Delta\sigma_{\text{drop}} , \quad (20)$$

such that the small difference in the box size, L, for different area fraction is absorbed into S. In Eq. (20), the stress drop is introduced as $\Delta\sigma_{\text{drop}} \equiv \sigma_q + \mu\Delta\gamma - \sigma_{q+1}$ $(q = 1, 2, \ldots)$, where $\mu \equiv (\sigma_q - \sigma_{q-1})/\Delta\gamma > 0$ is the shear modulus defined as the ratio of stress difference (in the previous strain step), $\sigma_q - \sigma_{q-1}$, to the strain increment, $\Delta\gamma$. Figure 6(a) displays the PDFs of avalanche-sizes, $P(S)$, where different symbols represent different values of the area fraction, ϕ. The power-law behavior, $P(S) \sim S^{-\tau}$ (dotted line), can be seen for any densities, while their tails are dependent on the area fraction. The exponent, $\tau = 1.35$, indicates the power-law of the complementary cumulative distributions, i.e. $F(S) \sim S^{-\nu}$ with $\nu = \tau - 1 = 0.35$ (which is used in the main paper). If we scale the avalanche-size and the PDFs as in Fig. 6(b), all the data for different densities are nicely collapsed. The collapsed data are well fitted by the power-law with a Gaussian cutoff, $P(S) \sim S^{-\tau} e^{-(S/S_g)^2}$ (red solid line), rather than the power-law with an exponential cutoff, $P(S) \sim S^{-\tau} e^{-S/S_e}$ (black solid line). Because the scaling exponent in Fig. 6(b) is given by $\lambda = 0.9$, the characteristic avalanche-sizes are scaled as $S_g, S_e \sim \Delta\phi^{0.9}$.

5.3 Dependence on the system size

We examine the system size dependence of the avalanche-size distributions. As shown in Sec. 5.2, the PDFs are described by the power-law with a cutoff function as

$$P(S) \sim S^{-\tau} f(S/S_c) , \quad (21)$$

where S_c is a characteristic size and $f(x)$ is a rapidly decreasing function (e.g. exponential or Gaussian). Note that Eq.

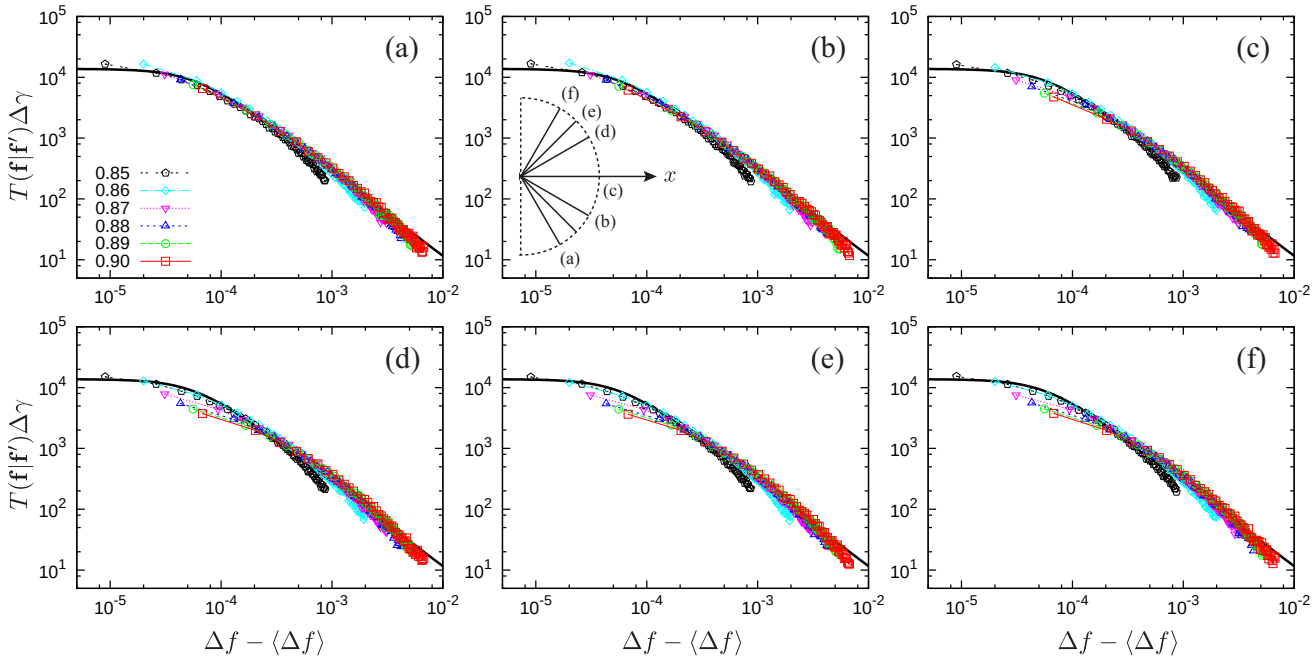

Figure 3: Transition rates for slip-avalanches, where $\Delta\theta = 0$ and the area fraction increases as listed in the legend of (a). We choose the contact angles as $\theta = \theta' = -\pi/3$ (a), $-\pi/6$ (b), 0 (c), $\pi/6$ (d), $\pi/4$ (e), and $\pi/3$ (f) which are measured from the x-axis as indicated in the inset of (b). The data for $\theta = \theta' = -\pi/4$ are given in the main paper.

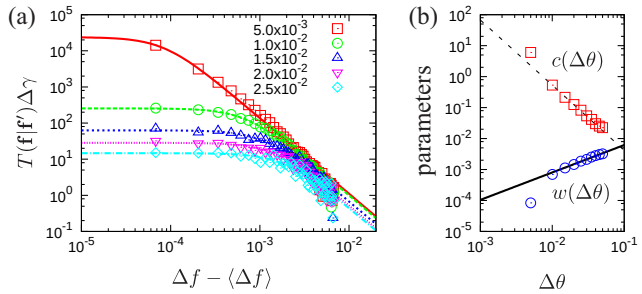

Figure 4: (a) Transition rates for slip-avalanches, where $\phi = 0.9$ is used and $\Delta\theta$ increases as listed in the legend. The lines are the q-Gaussian distributions, where the parameters, $c(\Delta\theta)$ and $w(\Delta\theta)$, are adjusted to data. (b) The parameters, $c(\Delta\theta)$ (squares) and $w(\Delta\theta)$ (circles), in the q-Gaussian distribution, Eq. (16). The dotted and solid lines are guides to the eyes ($c(\Delta\theta) \sim \Delta\theta^{-2.1}$ and $w(\Delta\theta) \sim \Delta\theta^{0.89}$, respectively).

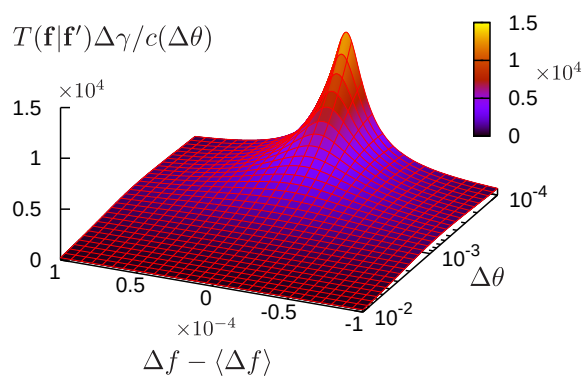

Figure 5: A three-dimensional plot of the transition rate scaled by $c(\Delta\theta)$, where the q-index, $w(\Delta\theta)$, and $c(\Delta\theta)$ are as in Figs. 3 and 4. The vertical axis and the color-bar should be multiplied by 10^4, while the horizontal axis, $\Delta f - \langle \Delta f \rangle$, should be multiplied by 10^{-4} (as indicated in figure).

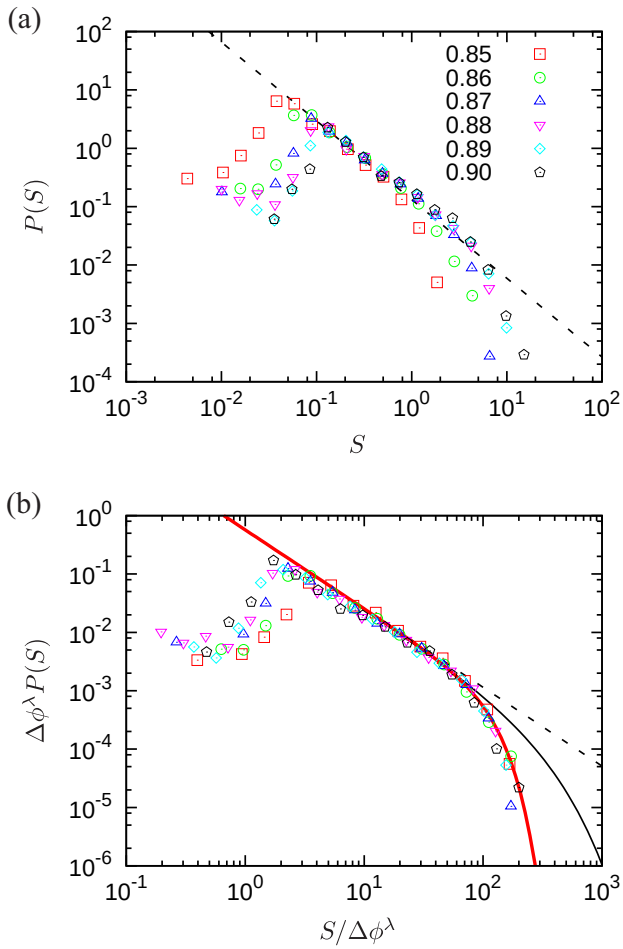

Figure 6: Double logarithmic plots of (a) the PDFs and (b) the scaled PDFs of avalanche-sizes, where different symbols represent different values of the area fraction, ϕ (as listed in the legend of (a)). The dotted lines indicate the power-law decay, $P(S) \sim S^{-\tau}$, with the exponent, $\tau = 1.35$. In (b), $\Delta\phi \equiv \phi - \phi_J$ with $\phi_J \simeq 0.8433$ is the proximity to jamming and the scaling exponent is $\lambda = 0.9$. The black and red solid lines represent $P(S) \sim S^{-\tau}e^{-S/S_e}$ and $P(S) \sim S^{-\tau}e^{-(S/S_g)^2}$, respectively, where the cutoff sizes are given by $S_e \simeq 257kd_0^2$ and $S_g \simeq 115kd_0^2$. Here, $N = 8192$ disks are used.

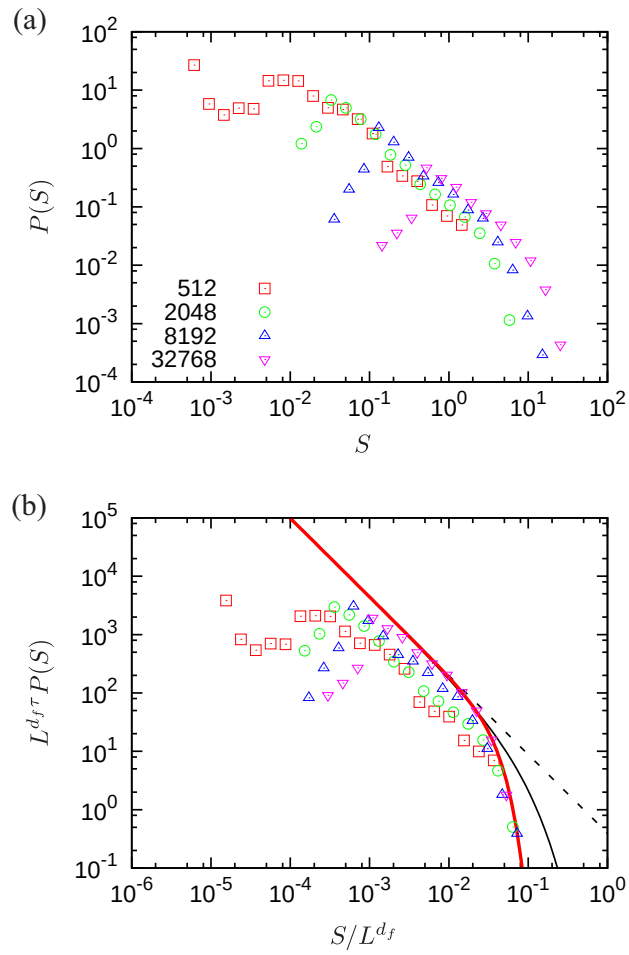

Figure 7: Double logarithmic plots of (a) the PDFs and (b) the scaled PDFs of avalanche-sizes, in the dense limit, $\phi = 0.9$, where different symbols represent the number of disks, N (as listed in the legend of (a)). In (b), L is the box size and the scaling exponent is given by $d_f = 1.2$. The dotted, black solid, and red solid lines are as in Fig. 6.

(21) can be rewritten as $S_c^{\tau}P(S) \sim (S/S_c)^{-\tau}f(S/S_c)$. Assuming that the characteristic size is scaled by the system size as $S_c \sim L^{d_f}$, we find the system size dependence of the PDFs as

$$L^{d_f\tau}P(S) \sim (S/L^{d_f})^{-\tau}f(S/L^{d_f}), \qquad (22)$$

where the scaling exponent, d_f, is called *fractal dimension*. Figure 7(a) shows the PDFs of avalanche-sizes with different system sizes (symbols). In Fig. 7(b), all the data can be collapsed if we use Eq. (22), where the scaling exponent, $d_f = 1.2$, is less than the spatial dimension, $d = 2$. We note that the data collapse in Fig. 7(b) is not so convincing and there is still a room for improvement in Eq. (22).